Proceedings of the 2007 IEEE/RSJ International
Conference on Intelligent Robots and Systems
San Diego, CA, USA, Oct 29 - Nov 2, 2007

Ultrasonic motor driving method for EMI-free image in MR image-guided surgical robotic system

Takashi Suzuki, Hongen Liao, Etsuko Kobayashi, and Ichiro Sakuma

Abstract— Electromagnetic interference (EMI) between magnetic resonance (MR) imager and surgical manipulator is a severe problem, that degrades the image quality, in MR image-guided surgical robotic systems. We propose a novel motor driving method to acquire noise-free image. Noise generation accompanied by motor actuation is permitted only during the "dead time" when the MR imager stops signal acquisition to wait for relaxation of protons. For the synchronized control between MR imager and motor driving system, we adopted a radio-frequency pulse signal detected by a special antenna as a synchronous trigger. This method can be applied widely because it only senses a part of the scanning signal and requires neither hardware nor software changes to the MR imager. The evaluation results showed the feasibility of RF pulse as a synchronous trigger and the availability of sequence-based noise reduction method.

I. Introduction

Conventional surgery consisted of three steps; preoperative surgical planning using diagnostic images, surgical operation by surgeons, and evaluation with postoperative images. Recently, intraoperative images, such as ultrasound, X-ray computed tomography (CT), and magnetic resonance (MR) image, have been used to identify the location of a target lesion and its displacement/deformation during the surgical procedure, and used to navigate surgical instruments. The intraoperative images also enable on-site evaluation of the surgical results. Surgeions can refresh the operatoion plan based on the results of intraoperative evaluation, that is impossible by the following-day evaluation. While imaging technology enhances surgeon's diagnostic ability and enables advanced diagnosis, surgical robot manipulators enhance the dexterity of surgeons and realize the higher quality of surgical operation. Some of them are commercialized and have been clinically applied in neuro, orthopedic, cardiac, and abdominal surgery [1]. Thus, integration of intraoperative images and surgical manipulators will lead to excellent surgical operations.

A. Problems in MR image-guided robot manipulator

MR imaging is one of the most attractive modalities because of its remarkable features: nonradiative, noninvasive, and advanced imaging such as angiography and temperature mapping. There are, however, many difficulties in collaboration between an MR scanner and surgical manipulators.

Magnetic material are used for most of mechanical parts and electromagnetic (EM) motors. They, however, cannot be used under or beside the high magnetic field of MR scanner because they could be a hazard by being attracted by the magnetic field. The existence of matnetic material also can be a problem because the homogeneity of the static magnetic field of the MR scanner is distorted. It leads to distortion of the acquired image. In addition, a surgical manipulator must not emit EM noise because noise degrades the image quality. MR scanners are weak against EM noise because the MR scanner is a very sensitive sensor that receives minute EM signals from protons inside the body.

Thus, an MR image-guided surgical manipulator is required to meet a series of specifications for safe operation and good image quality. It must be compatible with MR Imager (MRI). "MRI compatible". Chinzei, et al., quoted the definition of MRI compatibility from [2] as follows; 1) it is MR safe, 2) its use in the MR environment does not adversely impact the imaging quality, 3) it performs its intended function when used in the MR environment according to its specifications in a safe and effective manner [3]. Responding to these requirements, limited MRI compatible materials, actuators, and sensors are used in the magnetic field of an MR scanner. Engineering plastic, ceramics, titanium and aluminum are used instead of iron and stainless steel. In place of EM motors, for example, piezoelectric ultrasonic motors [3], [4], [5], [6] and hydrostatic transmission or pneumatic actuators [7], [8] are used. Optical position sensors are used to eliminate electrical noise [9], [10].

Although some researchers succeeded in manufacturing pneumatic actuator for MR-compatible manipulator [11], [12], they are not commercially available as a stand-alone actuator. Ultrasonic motor is the most widely used MR-compatible actuator [13]. The ultrasonic motor has various advantages; compact and light weight, holding torque without a brake. The body of ultrasonic motor body is MRI compatible, but EM noise is generated during motion. Because the EM interference degrades image quality, image acquisition and motor actuation could not be realized simultaneously. While Chinzei, et al., showed no significant degradation of images when the actuator was located near the isocenter of scanner, Koseki, et al., showed the image noise caused by motor actuation. In the authors' preliminary experiment, the image degradation by motor actuation was also observed. In some cases, actuation of ultrasonic motor

This work is partially supported by "Research on medical devices for analyzing, supporting and substituting the function of human body" funded by Ministry of Health, Labour and Welfare.

T. Suzuki is with Faculty of Advanced Techno-Surgery (FATS), Institute of Advanced Biomedical Engineering and Science (ABMES), Tokyo Women's Medical University, 8-1, Kawada-cho, Shinjuku-ku, Tokyo, 162-8666, Japan takashi_suzuki@ieee.org

H.Liao, E.Kobayashi, I.Sakuma are with Graduate School of Engineering, The Univ. of Tokyo, 7-3-1, Hongo, Bunkyo-ku, Tokyo, 113-8656, Japan. {liao, etsuko, sakuma}@bmpe.t.u-tokyo.ac.jp

1-4244-0912-8/07/$25.00 ©2007 IEEE.

results in no image degradation, but the noise problem cannot be ignored because the ultrasonic motor surely emits EM noise. Responding to the noise issue, two solutions are usually employed.

One is distance separation. Actuators are located far away from scanner or set up outside the MR room. Motion of the actuator is transmitted via mechanical elements such as linkages or cable/belt-driven mechanisms, which results in increased size and torque loss during transmission.

The other solution is to shut down the noise source. Actuators are powered off during scanning so as not to interfere with image acquisition. The first MR image-guided manipulator for stereotactic neurosurgery presented by Masamune, et al., employed this measure because they had no necessity of actuation during image scanning [4]. If organs are temporarily static, realtime image-based navigation is not necessary. However, when the target is a deformable and easy to shift, frequent scanning is required. Repetition of shutdown and restart of the system may elongate the operating time. Moreover, nonsimultaneous imaging cannot eliminate time lags between image-based motion planning and motor actuation.

B. Examples of realtime imaging in MR image-guided radiofrequency ablation (RFA) therapy

RFA therapy is a minimally invasive technique to eliminate tumor tissue by inserting a needle-shape electrode into the tumor lesion and by applying radiofrequency current to the tumor via the electrode to heat and ablate the tissue. In RFA therapy, realtime MR imaging is useful for precise needle placement, temperature mapping of ablated tissue, and intraoperative evaluation of the necrosis region. Because radiofrequency current for ablation causes interference with the imaging signal, the acquired image was affected by noise and results in a so-called "sandstorm" image. Some researchers have tried to acquire noise-free images during ablation therapy.

Oshiro, et al., used a bandpass filter to eliminate the RFA generator's noise and to receive only the imaging signal [14]. This method realized noise-free imaging. However, if the frequency band of the noise overlaps that of the imaging signal, this technique does not work.

Zhang, et al., switched the RFA generator on and off to eliminate the interference [15]. During the sampling time of imaging sequence, the RFA generator stops not to disturb the scanning. After the sampling time has passed, ablation begins and continues until the next sampling time. This method also contributed to acquiring noise-free images. MR imager, however, outputs a special command signal as a switching trigger to show the timing of sampling time. This measure requires modification of scanning sequence and cannot be always applied depending on the manufacturers of MR scanncer.

C. Objective

The purpose of this study is to realize realtime image acquisition and motor actuation simultaneously for MR image-guided robot surgery. We propose a novel MR image-compatible motor control method, that is manufacturer-independent to allow wide application regardless of the manufacturer of the MR imager.

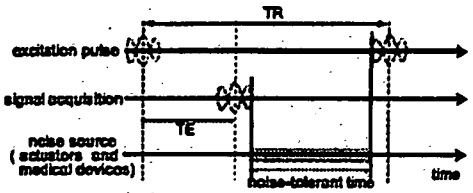

Fig. 1. Basic pulse sequence of MRI and dead time to wait relaxation of protons (noise-tolerant time).

II. METHOD

A. Basic principle

A pulse sequence in MR image acquisition generally repeats the following operation: 1) a series of excitation radiofrequency (RF) pulses is radiated to protons in the selected slice; 2) at the time when the echo time (TE) has passed, echo signals are received by the scanner; 3) the scanner waits for relaxation of protons before the next excitation.

In this study, we use the time period, the so-called "dead time," waiting for the relaxation of protons. The scanner does not receive any signal in dead time, so, of course cannot receive noise; thus, a noisy signal has no effect on image quality. We call this time period the "noise-tolerant time" (Fig. 1). Pseudo-simultaneous image acquisition and manipulation are available without interference if the motor is actuated only during the noise-tolerant time.

This technique can solve the problems in the former studies; clear images are available even if the bandwidth of the noise overlaps that of the image signal, and the operation time would not be elongated by switching between image scan and motor actuation because the motor is actuated not "between" but "during" imaging.

Here we need a technique to control the MR system and motors synchronously on an appropriate time schedule because motor actuation must be completed during the noise-tolerant time. As mentioned above, Zhang, et al., used a timing signal from the MR scanner as trigger [15], but this cannot be widely applied because the timing signal is not always available depending on the manufacturer of the MR system.

We propose a novel synchronous method that does not use an internal timing pulse of the MR system. We use an RF pulse in the MR scanning sequence as a synchronous trigger. Repetition time (TR) is the time unit to be repeated in a scanning sequence. As an RF pulse is radiated at the beginning of TR, we can recognize the start point of each TR, so RF pulse can be used as a synchronous trigger to represent the start point of the TR. Consequently the MR system and the manipulator can share a common time scale, and synchronous control between them can be realized.

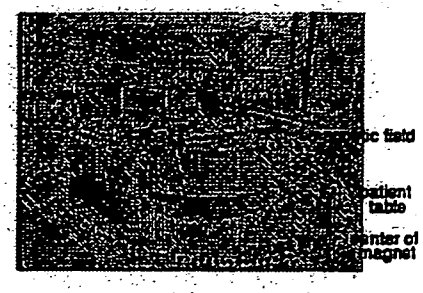

Fig. 2. MR imager (custom order for experimental setup).

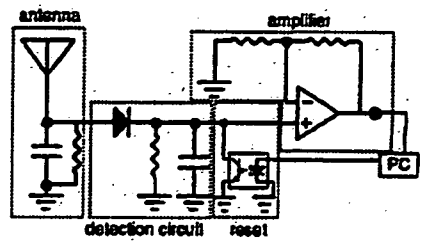

Fig. 3. RF pulse wave conditioning circuit for detection by computer.

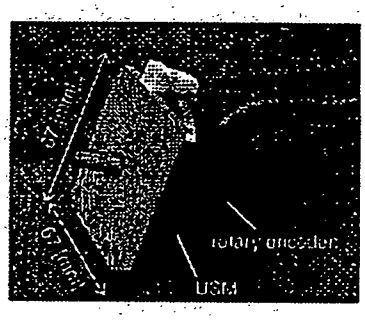

Fig. 4. Nonmagnetic piezo-electric ultrasonic vibration motor (Shinsei Corporation Inc., Japan).

As a receiver of the RF pulse, we developed a prototype external antenna. It is independent of the MR system and widely adaptable to any type of system. As another advantage of using the RF pulse as a synchronous trigger, it is radiated at every excitation of selected slices and synchronization will be conducted frequently, so that high accuracy of synchronization is guaranteed.

B. System configuration

For the realization of noise-free image acquisition under motor actuation noise using RF pulse synchronization, the system consists of four subsystems; MR system, the RF pulse receiving antenna, the surgical manipulator, and the computer.

1) MR imager: In this study, we used an open-configuration permanent magnet MR system with 0.2 T magnetic field (a custom-made prototype for our experimental setup) (Fig. 2). We did not use any scanner-specific functions. This means that our method can be applied widely to current clinical MR systems.

2) RF pulse receiving antenna: An original antenna was prototyped using a parallel resonance circuit with inductance and capacitance. The resonance frequency (f_0) of protons under the 0.2 T magnetic field (B_0) is 8.5 MHz from Larmor's equation:

$$\begin{cases} f_0 = \frac{\gamma}{2\pi}|B_0| \\ \frac{\gamma}{2\pi} = 42.6 \times 10^6 Hz/T \end{cases} \quad (1)$$

The antenna was connected to the computer to detect the RF pulse signal. We do not have to recognize the accurate waveform, but to know just start point of each TR. We adopted waveform-conditioning circuit to change analog waveform to digital pulse (RF pulse on/off) using detection circuit and amplifier. The schematic view of the circuit is shown in Fig. 3.

The RF signal is input into a detection circuit to obtain an envelope curve, and then into an amplifier circuit. The resistor at the detection circuit delayed the attenuation of the signal so that the computer could detect the RF pulse signal easily even if the duration time of the RF pulse was short. In the amplifier circuit, the signal was amplified up to 5 V so the binary signal was compatible with the computer. In the computer, we used a digital input/output circuit board (PCI-2726C, Interface Corporation, Japan) to detect the input RF signals.

3) Surgical manipulator: The final target of this study is to realize simultaneous control of the MR system and manipulation; to acquire noise-free images and drive a robot manipulator guided by the realtime image. The limited purpose of the present study, however, is the feasibility evaluation of synchronous control of MR system and an actuator without electromagnetic interference. Thus, we used an actuator as the controllable object and as a noise source instead of prototyping a surgical manipulator. We adopted a nonmagnetic piezoelectric ultrasonic motor with rotary encoder and its driver unit (USR60-E3N and D6060E, Shinsei Corporation Inc., Japan), which is widely used in MRI-compatible surgical manipulators[5], [7](Fig. 4). The motor was controlled using the above-mentioned digital input/output board (PCI-2726C, Interface Corporation, Japan) for motion command, a DA converter board (PCI-3338) for speed control, and an encoder counter board (PCI-6201) for rotational angle sensing.

4) Control computer: A computer (CPU: Pentium III, 500 MHz, RAM: 384 MB) was implemented to integrate above subsystems. The operating system was originally built using Red Hat Linux 9 (kernel version 2.4).

The task of the computer was to manage subsystems. When a RF signal is received , the computer recognizes it as the start point of TR and resets its timer, then waits until TE has passed. After acquisition of the echo signals by MR scanner, the computer actuates the motors during the noise-tolerant time. When the time for the next RF pulse is approaching, the computer stops the motors and waits for the next RF pulse.

In this study, parameter values of TR, TE, and noise-

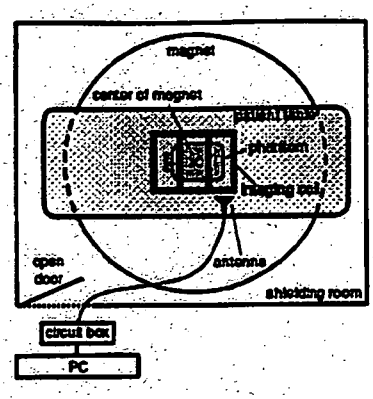

Fig. 5. Experimental setup for feasibility test of RF pulse detection.

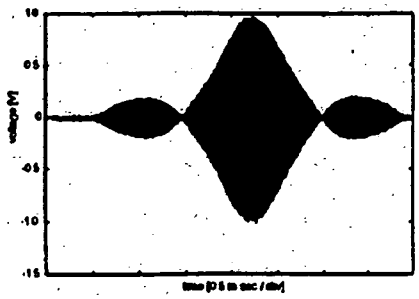

Fig. 6. Detail view of received RF pulse.

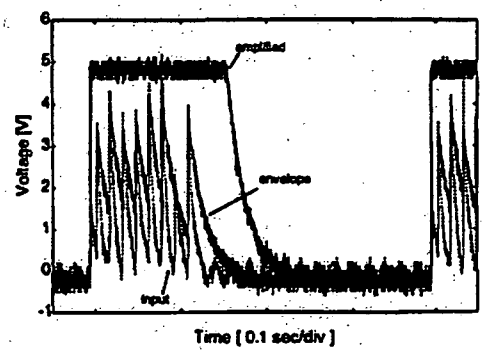

Fig. 7. Received RF pulse and wave conditioned results.

tolerant time were supplied to the computer manually. We plan to supply them semi-automatically using the Digital Imaging and Communication in Medicine (DICOM) data.

III. Evaluation Experiments

A. Feasibility of RF pulse as a synchronous trigger

The first experiment was conducted to evaluate the feasibility of RF pulse as a synchronous trigger. The experimental setup is shown in Fig. 5. At the center of the magnet, a head coil and a cylindrical imaging phantom ($NiCl_2$ 18 m mol/l and NaCl 0.7 weight/volume % solution in a plastic bottle) were positioned. The RF pulse-receiving antenna was attached using adhesive tape 160 mm from the center of the magnet. The computer and circuit box were also located outside the MR room not to cause image degradation.

The imaging parameters are as follows; scanning sequence: fast spin echo (FSE); TR/TE: 400/15 ms; flip angle: 90 degree; slice thickness: 8 mm; resolution:128×248; field of view (FOV):250×250 mm^2. The FSE-specific parameters were: echo space (ESP): 15 ms; echo train length (ETL): 8. We measured the signals at three points; 1) the raw RF pulse signal wave received by the antenna, 2) the envelope , and 3) the amplified envelope.

Figure 6 shows a detailed view of the received RF pulse. The application utility to measure frequency of the wave in the oscilloscope showed that the frequency of the observed wave was 8.5 MHz, equivalent to the Larmor frequency in a 0.2 T magnetic field. Figure 7 shows the three measured waveforms. The raw waveform was conditioned to a pulse wave, and the conditioned wave was receivable by the computer.

B. Image quality with and without the proposed method

We implemented a simple experimental setup and actuated the ultrasonic motor under the magnet during scanning, and compared MR images and signal-to-noise ratios (SNR).

The experimental setup is shown in Fig. 8. In addition to the setup in Fig. 5, the ultrasonic motor was located 350 mm from the center of the magnet. The cable of the ultrasonic motor was also led to outside. The ultrasonic motor driver unit box was located outside the MR room. The imaging parameters were as follows: scanning sequence: FSE; TR/TE: 400/15 ms; flip angle: 90 deg; slice thickness: 8 mm; image matrix: 128×128; Field of View: 250×250 mm^2. The FSE-specific parameters were: ESP: 15 ms; ETL: 8. The image acquisition time was 6.4 s.

A schematic view of the pulse sequence is shown in Fig. 9. The control software; 1) waits for reception of the RF pulse, 2) resets the timer when RF pulse is received, 3) actuates the motor (100 ms) after TE (120 ms) and additional time to avoid interference (80 ms), 4) stops the motor 100 ms before the next RF pulse and waits for the next RF pulse. TR was repeated 16 times in one image acquisition, and in each TR we spent 100 ms of noise-tolerant time for motor actuation. The actuation time can be longer, but we simply set the time period shorter for this preliminary trial to avoid interference between the image signal acquisition and motor actuation.

Figure 10 shows the results of imaging; (a) only the phantom with the door closed for reference, (b) only the phantom with the door open, (c) the phantom with antenna and motor (power was off), (d) the phantom with antenna and motor (power was on, but motion was stopped), (e) the phantom with motor actuated with synchronous control, and (f) the phantom with motor actuated without synchronous control. For quantitative evaluation, we calculated the signal-to-noise ratio (SNR) using the following equation (Fig. 11):

$$SNR = I_{center}/SD_{corners} \quad (2)$$

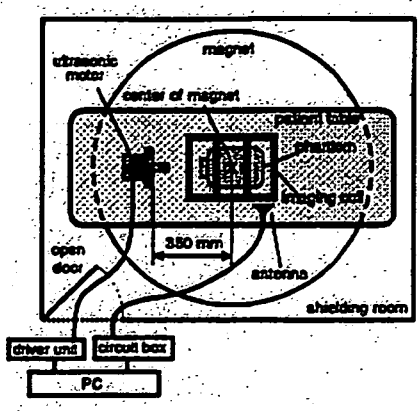

Fig. 8. Experimental setup for image degradation by noise of motor.

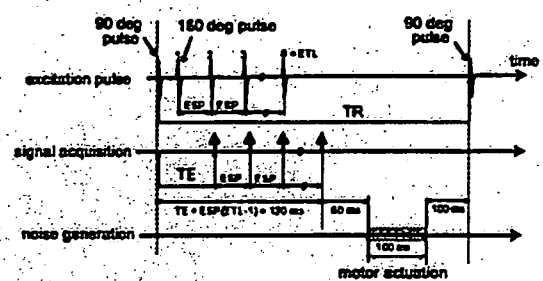

Fig. 9. Pulse sequence; experimental setting for noise evaluation.

I_{center} is the average intensity of the target region (E) at the center of image, and $SD_{corners}$ is the average of the standard deviation of the intensity at the corners (A, B, C, D) of the image. The diameter of the circular region was 19 pixels. The location of the imaging phantom and the circular regions was fixed during evaluation. Image acquisition was repeated five times for each condition, and the average, standard deviation, and reduction rate to (a) is shown in Table I.

Comparing (a) and (b), open door showed no apparent degradation of image quality and SNR reduction of 3%. This is because the phantom is shown as a high-contrast object and background noise is relatively small and ignorable.

The difference between (b) and (c) was caused by the antenna and the ultrasonic motor near the imaging region. Though no apparent degradation of image was found, the SNR decreased by 8%. The cause was thought to be noise from outside MR room introduced through the cables of the antenna and motor.

Comparison between (c) and (d) shows the difference when we turn on and off the motor driving unit. No apparent noise or decrease in SNR were found although more degradation had been expected when power was turned on.

Lastly, we compared (d) with (e) and (f). While (e) showed no noise in the image, (f) could not be used as an image. In terms of SNR, (d) and (e) are almost the same, but (f) has decreased by 93%.

These results show that our novel MRI-compatible method

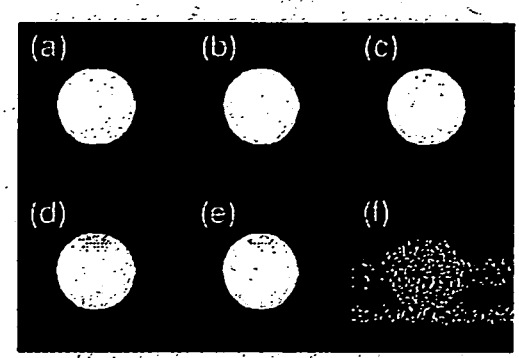

Fig. 10. Results of image acquisition under various conditionds.

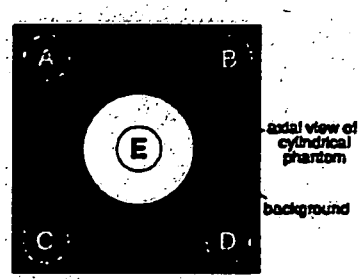

Fig. 11. Signal-to-noise ratio calculation method in an image.

achieved noise-free image acquisition during motor actuation.

IV. Discussion

The results of evaluation tests show that the synchronous control between MR scanner and ultrasonic motor decreased SNR less than 8% while continuous control decreased 93%. Here, we need a certain standard to evaluate the decrease of SNR. We repeated image acquisition 100 times under the condition of (a). The SNR varies almost 10% around the average value even if the imaging condition was fixed (Table. II). From this result, as we concluded that approximately 10% change of SNR was acceptable.

This method can solve some problems in the MR image-guided surgical manipulator. In the former studies, ultrasonic motors were located far away from MR scanner to avoid interference, and rotational torque was transmitted via mechanical parts, leading to increased size of manipulator and torque loss. As our method enables motor driving near magnet, we can eliminate the transmission mechanism to miniaturize the manipulator. A compact space-saving manipulator is easy to setup and handle, and enables easy access to the patient during operation. We also have no necessity of shutting down the actuator driver during scanning. Repetition of shutdown and restart of the system is not necessary.

A limitation of this method is the problem of trading off between scanning speed and noise-tolerant time for motor actuation. For precise tracking of moving soft tissue, the scanning time should be shorter and a higher refresh rate is desirable. The refresh rate, however, cannot be so

TABLE I

SIGNAL TO NOISE RATIO.

Image	SNR	Normalization
(a)	146.5 ± 5.5	100.0
(b)	142.5 ± 3.3	97.2
(c)	135.0 ± 3.3	92.1
(d)	135.9 ± 6.6	92.8
(e)	135.9 ± 3.2	92.8
(f)	10.2 ± 1.4	7.0

TABLE II

VARIATION OF SIGNAL-TO-NOISE RATIO UNDER THE SAME CONDITIONS.

	SNR	
average±S.D.	204.2 ± 7.0	
max	221.3	+8.4 % to average
min	185.9	-9.0 % to average

high because high-speed scanning (shorter scanning time) leaves less noise-tolerant time for motor actuation. Because a certain length of time is necessary for start-up response, acceleration, and deceleration in the control of surgical manipulator, we cannot use the synchronous method with some high-speed sequences in current interventional MRI therapy, such as the multiplanar technique and echo planar imaging technique.The pulse sequence in III. Evaluation experiments was just one example for applying the proposed method. It was neither optimized for a clinical application nor the only example to apply the proposed method. Preset pulse sequences in MR systems are optimized for each target such as brain, heart, liver, spine, and for each purposes, T1 weighted, T2 weighted, brain function imaging, angiography, and temperature mapping. Thus, current clinical pulse sequences are not necessarily appropriate for MR image-guided surgical manipulator.

As mentioned above, the proposed method does not aim to complete all procedures under MR image guidance, but is intended to check the positioning of the target and surgical instruments. An example would be high-accuracy needle insertion to a targeted liver tumor with short-time breath holding in RFA therapy under MR image navigation.

Thus, new types of pulse sequences should be developed and optimized for MR image-guided robot surgery to realize higher refresh rates and longer noise-tolerant times simultaneously. Requirements for noise-tolerant time will change depending on the situation, in other words, the required length of the noise-tolerant time. It will be specified by the mechanical configuration of manipulator, performance of the actuator, the movement range and frequency of the target organ, refresh rate and quality of MR image, and so on. New pulse sequences for MR image-navigated robot surgery will maximally use the advantages of the proposed MRI compatible imaging method.

V. CONCLUSION

This study proposed a novel MRI-compatible method. It realizes both noise-free image acquisition and motor actuation pseudo-simultaneously by synchronous control of the MR scanner and motor, considering the noise-tolerant time in the pulse sequence. As a synchronous trigger to identify the start point of TR, the RF pulse signal in a scanning sequence is adopted.

The results of evaluation tests showed that 1) the RF pulse can act as a synchronous trigger, 2) the newly proposed MRI-compatible motor control method realizes noise-free image acquisition, not being affected by electromagnetic noise from the driving motor.

To the authors' best knowledge, this is the first report about the noise reduction method based on pulse sequence in the field of MR image-guided surgical manipulator. Moreover, RF pulse is firstly adopted as a synchronous trigger between MR scanner and surgical manipulator, not internal timing signal from MR scanner. It is a very simple, inexpensive, and manufacturer-independent, so that widely applicable to any MR system.

As a future work, for the best application of proposed MRI compatible method, we must develop new pulse sequences optimized for intraoperative image navigated surgical robot manipulators.

REFERENCES

[1] G.H.Ballantyne. Robotic surgery, telerobotic surgery, telepresence, and telementoring review of early clinical results. *Surg. endosc*, 16(10):1389–1402, 2002.

[2] GE Medical systems. MR safety and MR compatibility: Test guidelines for signa SP^{TM}, version1.0., 1997.

[3] K. Chinzei, et al. MR compatibility of mechatronic devices: Design criteria. In *Proc. of 2nd Int'l Conf. on Medical Image Computing and Computer-Assisted Intervention (MICCAI'99)*, pages 1020–1031, 1999.

[4] K. Masumune, et al. Development of an MRI-compatible needle insertion manipulator for stereotactic neurosurgery. *J Image Guid Surg*, 1(4):242–248, 1995.

[5] Y. Koseki, et al. Endoscope manipulator for trans-nasal neurosurgery, optimized for and compatible to vertical field open MRI. In *Proc. of 5th Int'l Conf. on Medical Image Computing and Computer-Assisted Intervention-MICCAI2002*, pages 114–121, 2002.

[6] B.T. Larson, et al. Design of an MRI-compatible robotic stereotactic device for minimally invasive interventions in the breast. *Trans ASME J Biomech Eng*, 126(4):458–465, 2004.

[7] D. Kim, et al. A new, compact MR-compatible surgical manipulator for minimally invasive liver surgery. In *Proc. of 5th Int'l Conf. on Medical Image Computing and Computer-Assisted Intervention (MICCAI2002)*, pages 99–106, 2002.

[8] S.P. DiMaio, et al. A system for MRI-guided prostate interventions. In *Proc. of The First IEEE/RAS-EMBS Int'l Conf. on Biomedical Robotics and Biomechatronics (BioRob 2006)*., pages 68–73, 2006.

[9] F. Tajima, et al. Development of MR compatible surgical manipulator toward a unified support system for diagnosis and treatment of heart disease. In *Proc. of 5th Int'l Conf. on Medical Image Computing and Computer-Assisted Intervention (MICCAI2002)*, pages 83–90, 2002.

[10] R.Riener, et al. fMRI-compatible electromagnetic haptic interface. In *Proc. of the 2005 IEEE Engineering in Medicine and Biology Society, 27th Annual Conference*, pages 1106–1109, Shanghai, September 2005.

[11] http://www.innomedic.de/.

[12] D. Stoianovici, et al. A new type of motor: Pneumatic step motor. *IEEE/ASME Transactions on Mechatronics*, 12(1):98–106, February 2007.

[13] R. Gassert, et al. Actuation methods for applications in MR environments. *Concepts in Magnetic Resonance Part B: Magnetic Resonance Engineering*, 29B(4):191–209, 2006.

[14] T. Oshiro, et al. Reduction of electronic noise from radiofrequency generator during radiofrequency ablation in interventional MRI. *J. comput. assist. tomogr.*, 26(2):308–316, 2002.

[15] Q. Zhang, et al. A method for simultaneous RF ablation and MRI. *J. magn. reson. imaging*, 8(1):110–114, 1998.

HIFU Tumor Therapeutic System has been approved for the treatment of a variety of tumors such as liver cancer and breast cancer, etc. in China in November 2004. Currently 3 systems are working there. With the aid of the new ultrasound-guided HIFU system of Sonic CZ901, the focused ultrasound treatment will become more accessible to the physicians and patients with benign or malignant tumors. The new HIFU system has the possibility to be suitable HIFU for improving for rectal and liver cancer with remaining ribs.

WS4-4
Augmented reality navigation guided laparoscopic nephrectomy

Hidekazu Takiuchi[1], Atsushi Nakao[1], Masao Tanooka[2]
[1]Department of Urology, Nishinomiya Municipal Central Hospital, Japan,
[2]Department of Central Radiology, Hyogo College of Medicine, Japan

[Purpose] The key of successful laparoscopic nephrectomy is a treatment step of renal vessels. So we investigated the efficacy of augmented reality in laparoscopic kidney resection in regard to blood loss, operative time and complications. [Methods] In order to navigate surgeons, 3-dimensional volume rendering images of renal vessels including their brunches, pancreas, adrenal gland and tumor mass were created in advance of operation based on the result in computerized tomography examinations. Those images were augmented on surgical views on sub-monitor which duplicated surgical main monitor images. A navigator adjusted the view angle and the size of volume rendering images to surgical views. The operators treated renal vessels using augmented reality images as a guide. Augmented reality navigation guided laparoscopic nephrectomy was performed on five cases with renal or ureteral cancer. We compared the data of navigation surgery using augmented reality with those without it. [Results] Operative time ranged from 215 minutes to 360 minutes. Blood loss was below 50 ml in all cases, and no major complication was experienced. In comparison of navigation surgery with or without augmented reality, operative time in augmented reality navigated surgery group was significantly shorter than that in one without augmented reality. There was no significant difference in blood loss between two groups. [Conclusions] Augmented reality made it possible to perform safe and bloodless surgery in laparoscopic nephrectomy.

WS4-5
Electromagnetic tracking of a guidewire for angiographic interventions: A phantom study

Rudolf Stoffner[1], Neil Glossop[2], Gerlig Widmann[1], Christoph Hinterleithner[1], Thomas B. Lang[1], Werner Jaschke[3], Reto J. Bale[1]
[1]University Hospital of Diagnostic Radiology, Department of Diagnostic Radiology I, Innsbruck Medical University, Austria,
[2]Traxtal Inc., Toronto, ON, Canada,
[3]University Hospital of Diagnostic Radiology, Innsbruck Medical University, Austria

Purpose To evaluate the spatial accuracy of a pre-release of the PercuNav™ electromagnetic (EM) navigation system (Traxtal Inc., Toronto, ON, Canada) for image guided positioning of a guidewire in a plastic phantom of a human torso. Methods Twenty-five metal beads representing artificial target points were glued onto the outer wall of water-filled tubes that mimicked blood vessels. Additional registration markers were mounted to the phantom's surface. A CT scan with 1 mm slice thickness was obtained and the data was sent via the hospital PACS system to the navigation system. A surface-mounted patch was attached externally to dynamically reference the phantom. After registration (mean fiducial registration error <1 mm), a guidewire (diameter: 0.89 mm, length: 1750 mm) containing an electromagnetic tracking sensor coil at its tip was advanced until the target fiducial was visible in the reformatted axial cross-section provided by the navigation system. At each target position a CT was performed and the Euclidean distance from the tip of the guidewire to the target marker was measured and compared with the distance given by the navigation system. All target points were localized twice. The difference between *distance to the target on the postoperative control-CT* and the *distance to the target displayed on the navigation* system was calculated. Results The guidewire position was evaluated in 50 locations, resulting in an overall target localization error (TLE) of 1.53 mm (standard deviation 1.2 mm, maximum 3.9 mm). Discussion Electromagnetic navigation enables accurate tracking of instruments inside the body that is not limited by the line-of-sight restrictions affecting optical tracking systems. The low TLE measured in this study is likely to increase in clinical use due to a combination of errors including to registration and uncompensated motion (respiration, cardiac induced motion), but accuracy should be acceptable for many interventions.

WS4-6
Precise micro-laser ablation system with intra-operative fluorescence image guidance

Ichiro Sakuma[1], Masafumi Noguchi[1], Eisuke Aoki[1], Hongen Liao[1], Etsuko Kobayashi[1], Shigeru Omori[2], Yoshihiro Muragaki[3], Katsushige Nakamura[3], Hiroshi Iseki[3]
[1]Department of Precision Engineering, School of Engineering, The University of Tokyo, Japan,
[2]R&D Center, Terumo Corporation,
[3]Faculty of Advanced Techno-surgery, Institute of Biomedical Engineering and Science, Graduate School of Medicine, Tokyo Women's Medical University

Combination of intra-operative medical imaging such as intra-operative MRI, surgical navigation system, and surgical robot, will become important technology for the minimally invasive surgery in the future. Several technologies should be developed for this purpose. One of promising intra-operative imaging modalities is optical imaging such as fluorescence imaging. Recent progress in selective tissue staining dyes makes it possible to obtain important pathological information by intra-operative optical measurement. We combined system of tumor detection by 5-ALA-induced PpIX fluorescence and precise ablation by micro laser for the first time, with an automatic focusing and robotic scanning mechanism for the brain surface.
We developed a combined system of tumor detection by 5-ALA-induced PpIX fluorescence and precise ablation by a micro laser for the first time, with an automatic focusing and robotic scanning mechanism for the brain surface. 5-ALA accumulates on tumors to be metabolized to become PpIX

that is fluorescent. Intra-operative detection of 5-ALA induced PpIX fluorescence provides useful information for tumor detection. The wavelength of the micro laser is 2.8 μm close to the absorption band of water. This laser is effective only on the surface of brain tissue, enabling precise ablation at the boundary between tumor and normal tissue identified by intra-operative 5-ALA induced fluorescence. Combination tests of the fluorescence measurement and the laser ablation were performed. The target was the surface of a porcine brain exposed by craniotomy under anesthesia. Before the experiment, 5-ALA was administrated in sufficient quantities to accumulate on a normal brain tissue and metabolize to become PpIX. A half of the measurement area was covered with dura matter to stop fluorescence signal emission. It was possible to extract the area with fluorescence appropriately from the measurement data, and the micro laser with automatically scanning selectively ablated the extracted area.

WS4-7
Fully automated registraton of intraoperative Computer Tomography image data

Georg Eggers[1], Bodo Kress[2], Joachim Muehling[1]
[1]Oral and Cranio-Maxillofacial Surgery, Heidelberg University, Germany,
[2]Department of Neuroradiology Heidelberg University Germany

Introduction: Patient to image registration is a prerequisite for any kind of image guided surgery, be it navigation systems, augmented reality or robotics. Standard registration methods are based on pair-point registration or surface matching algorithms. We present a new method for fully automated registration of intraoperative Computer tomography (CT)-image data to the patient. The registration accuracy of this method for navigation in craniofacial surgery was evaluated. Materials and methods: The concept for fully automated registration of patient and CT-image data is based on the idea, that the position of the patient and the position of the gantry of the CT scanner are tracked in the process of image data acquisition, using the infrared tracking system of the navigation system. With the image plane of the gantry being calibrated to the tracking marker, registration of the acquired image data fully is performed immediately and fully automatically. Accuracy evaluation was performed in a phantom study: a plastic phantom skull was equipped with 40 titanium target markers in the face and the neurocranium. Registration of CT-data was performed with 4 different configurations of the tracking system. The accuracy of identifying the artificial skull-mounted targets, using the navigation system after the automated registration, was determined for each registration. Results: The average target registration error was always better than 1.5 mm. Inaccuracies were distributed homogeneously over the phantom. The measured targeting accuracy would always have been sufficient for image-guided surgery of any region of the skull and face. Conclusions Fully automated registration of intraoperatively obtained data from a tracked CT gantry is an accurate registration method. It is now in routine patient care use and has proven its value.

WS4-8
Innoguide - A new device for stereotactic brain biopsy under continuous MR-imaging

Uwe Spetzger[1], Gerd Winkler[1], Sebastian Arnold[2], Ulrich Altdoerfer[1], Peter Reimer[2], Thomas Remmele[3]
[1]Neurosurgery, Klinikum Karlsruhe, Germany,
[2]Department of Radiology, Klinikum Karlsruhe, Germany,
[3]Innomedic, Herxheim, Germany

Introduction: Stereoactic biopsy of cerebral lesions is a routine procedure in neurosurgery. A frame is fixed at the patients head and a CT or MR-scan is performed. These coordinates allow an exact localization within the brain and the trajectory planning to reach the target with the probe. The stereotactic strategy is not only used for diagnostic purpose like brain biopsy, the precise placement of catheters or electrodes also allow therapeutic regimens. Generally, in local anaesthesia a small burr hole is performed and a biopsy needle or electrode is placed into the planned target area. At present, various MR-tomographs are installed in operating theatres to allow neurosurgical procedures under radiological control. Our idea was to bring the whole stereotactic set-up into the MR suite, and not the MR into the OR. Methods: In an industrial scientific collaboration we developed a fully MR-compatible stereotactic frame. All components and materials fit into the gantry of a conventional high-field 1.5T machine. Therefore, the radiological control of the stereotactic procedure is possible in real-time. The movement and final positioning of the biopsy needle and the biopsy itself is visible on-line, due to ongoing MR-image acquisition during surgery. Results: The planning, the development and the construction of InnoguideTM is demonstrated. Initial tests, a phantom study as well as a feasibility study with a cadaver head are shown. Meanwhile, the first clinical results of our ongoing pilot study with 8 patients are available. Conclusion: The workflow of the whole stereotactic procedures is improved and it also enhance the precision and the safety for the patient.

WS4-9
A Realtime Navigation for Endoscopic Surgery based on multimodality medical imagings: Experiences with 30 clinical cases

Kozo Konishi[1], Masahiko Nakamoto[2], Yoshihiro Kakeji[3], Kazuo Tanoue[4], Hirofumi Kawanaka[3], Satoshi Ieiri[4], Ichiro Yoshino[3], Yoshinobu Sato[2], Takashi Maeda[1], Yoshihiko Maehara[3], Makoto Hashizume[4]
[1]Department of Future Medicine and Innovative Medica Information, Kyushu University, Japan,
[2]Division of Interdisciplinary Image Analysis, Osaka University Graduate School of Medicine,
[3]Department of Surgery and Science, Graduate School of Medical Sciences, Kyushu University,
[4]Center for Integration of Advanced Medicine, Life Science and Innovative Technology, Kyushu University

In the endoscopic surgical fields, more information which could be used intraoperatively is strongly demanded Three-dimensional reconstructed images are useful imaging modalities to assist the surgeon in endoscopic surgery. We expected a new magneto-optic hybrid 3-D sensor configuration, and have developed an augmented realigy navigation system using an accurate three dimensional sensory system that can be utilized in endoscopic surgery. The system has accommodated oblique endoscope, real time distortion correction of magnetic fields. We have established 'combined' navigation system. The complete system consists of a

07(II)-8

超音波凝固切開装置を搭載した多自由度屈曲鉗子における先端回転制御法のシミュレーションおよび評価

○吉村 雄祐[a], 遊尾 健[b], 小林 英津子[a], 伊関 洋[c], 中村 亮一[c], 佐久間 一郎[a]

[a]東京大学大学院工学系研究科, [b]東京大学大学院新領域創成科学研究科, [c]東京女子医科大学大学院医学研究科

Simulation and evaluation of control of tip-rotation intended for the multi-DOFs bending forceps equipped with Ultrasonically Activated Scalpel

Y. Yoshimura [a], T. Hasuo [b], E. Kobayashi [a], H. Iseki [c], R. Nakamura [c], I. Sakuma [a]

[a] *Graduate School of Engineering, The University of Tokyo, Tokyo, Japan*

[b] *Graduate School of Frontier Sciences, The University of Tokyo, Tokyo, Japan*

[c] *Graduate School of Medical Sciences, Tokyo Women's Medical University, Tokyo, Japan*

Abstract: Ultrasonically activated scalpels (USADs) are widely used in laparoscopic surgery to incise and coagulate tissue simultaneously. However, it is difficult for surgeons to manipulate a USAD and approach to a target tissue because it has only a linear shape and limits the degree of freedom. To solve this problem, we developed new bending forceps with a small USAD on their tip. In this report, we proposed a new motion planning of the developed forceps to achieve safe and easy operations for surgeons. We simulated the control of the rotation of their tip. As a result, the USAD blade followed the rotation of the body axis within less than 19.8 degrees when the angle between them was less than 45 degrees.

Key words: Ultrasonically Activated Scalpel, Minimally Invasive Surgery, Bending forceps, Control of tip-rotation

1. 背景

超音波凝固切開装置(Ultrasonically Activated Scalpel, 以下USAD) は, 止血と切開を同時に行うことができ, 同様の電気メスと比較し, 組織と患者に与える損傷が軽微であるといった利点をもち, 腹腔鏡下手術において盛んに使用されている.[1] しかし, 現在普及している USAD はすべて直線形状であり, 手術器具が腹腔上の挿入孔で拘束される腹腔鏡下手術においては満足な取り回しが可能であるとはいえない. また作動中のUSADのブレードが目標でない組織に誤って接触した場合に, 重大な事故となる危険性が指摘されている.

そこで, 本研究では, USAD の操作性を向上させることを目指し, 小型 USAD を先端に搭載した多自由度屈曲鉗子を開発し, その先端回転制御法について数値シミュレーションにより検討した.

2. 先端回転制御法

2.1. 多自由度屈曲鉗子

多自由度屈曲鉗子の屈曲・回転自由度の配置を決定するに当たり, 腹腔鏡下手術の術式を観察し, 術者はいかにして鉗子先端の位置, 姿勢の決定を行うかについて検討を行った. その結果, 暫定的に, 術者は鉗子先端操作において位置決め → 先端の回転というシーケンシャルな操作を行うという仮説を立てた. この場合, 回転自由度は屈曲自由度より先端側に位置することが重要となる. しかしながら, 機構の複雑さや先端部のサイズの観点から, 回転機構を先端部に実装することは困難を伴う. そこで Fig. 1 のように, 本体軸周り回転機構を2 自由度の屈曲関節より手元側に配置した 2.5 次試作機を製作した. この試作機に対し, 屈曲関節角を制御することで, 本体軸周り回転を手動で入力すると, USADブレードの方向を維持したまま, ブレード軸周りに入力角に応じて回転するという先端回転制御法を行う.[2]

製作した2.5 次試作機の鉗子直線部の径は 10 (mm), 長さは 370 (mm), 手元側および先端側の屈曲関節中心間距離 d は 13.4 (mm), 先端側の屈曲関節中心からUSADブレード先端までの距離は 73 (mm)である.

2.2. 制御方法

先端回転制御法において, 本体軸周り回転角が与えられたときの屈曲関節角を以下のように決定する. はじめに, Fig. 1 のように座標系{A}, {B}を設定し, 本体軸周り回転角をϕ, 手元側の屈曲関節角をθ, 先端側の屈曲関節角をψとおく. 次に, 目標とするUSADのブレードの方向Z_B が Fig. 2 のようにパラメータα, βで与えられた場合, 座標系{A}から見たZ_B は, {ϕ, θ, ψ}, および{α, β}のパラメータを用いて表すことができる. これらの関係式より, 屈曲関節角θ, ψは, α, β, ϕを用い次式で表される.

$$\theta = \tan^{-1}\left(\frac{\sin\alpha\cos(\phi-\beta)}{\cos\alpha}\right) \quad (1)$$

$$\psi = \sin^{-1}(\sin\alpha\sin(\phi-\beta)) \quad (2)$$

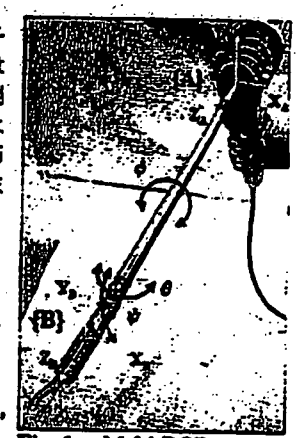

Fig. 1. Multi-DOFs bending forceps. 2.5th prototype.

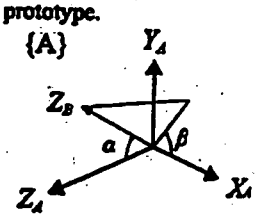

Fig. 2. Definition of positioning parameters α, β.

更に，先端回転制御法の評価のため，鉗子本体を本体軸周りに0からϕまで回転させたときのUSADブレード軸周りの回転角γを導出した．γは次式で与えられる．

$$f(\phi)=\tan^{-1}\left(\frac{\cos\theta\sin(\phi-\beta)}{\sin\theta/\sin\alpha}\right) \quad (3)$$

$$\gamma=f(\phi)-f(0) \quad (4)$$

先端回転制御法において，USADブレード軸周りの回転角γが，本体軸周り回転角ϕに追従することが理想的である．従って，それらの差分$\Delta\gamma=\gamma-\phi$を本制御法の評価項目とした．

3. 数値シミュレーション

はじめに，先端回転制御法において，USADブレードの方向Z_Bが維持されていることを確認するために，式(1), (2)より得られた屈曲関節角θ, ψを用い，順運動学を解き，本体軸周り回転角ϕを0 (deg)から360 (deg)まで10 (deg)刻みに変化させたときの手元側屈曲関節中心，先端側屈曲関節中心，USADブレード先端の位置を求めた．以下では，パラメータαを15 (deg)から75 (deg)まで1 (deg)刻みに，βを0 (deg)から360 (deg)まで1 (deg)刻みに変化させ，数値シミュレーションを行った．代表例としてFig. 3に，$\alpha=45$ (deg), $\beta=0$ (deg)の場合の計算結果を示す．ここで，手元側屈曲関節中心を原点にとって表示している．

次に，本体軸周り回転角ϕを0 (deg)から360 (deg)まで連続的に変化させたときの評価項目$\Delta\gamma$の変化を計算し，その変化における$|\Delta\gamma|$の最大値$|\Delta\gamma|_{max}$を求めた．代表例としてFig. 4に，$\beta=0$ (deg)の場合の$\Delta\gamma$の変化を示す．ここで，1は$\alpha=15$ (deg)，2は$\alpha=30$ (deg)，3は$\alpha=45$ (deg)，4は$\alpha=60$ (deg)，5は$\alpha=75$ (deg)の場合の結果を示す．$\alpha=15, 30, 45, 60, 75$ (deg)の場合，最大値$|\Delta\gamma|_{max}$は各々0.99, 4.1, 9.9, 19.5, 36.1 (deg)となる．更に，βを変化させたときの$|\Delta\gamma|_{max}$の変化をFig. 5に示す．ここで，1は$\alpha=15$ (deg)，2は$\alpha=30$ (deg)，3は$\alpha=45$ (deg)，4は$\alpha=60$ (deg)，5は$\alpha=75$ (deg)の場合の結果を示す．

4. 考察

Fig. 3に示されるように，先端回転制御法において，USADブレードの方向は維持される．ただし，手元側および先端側の屈曲関節中心間に距離$d=13.4$ (mm)が存在するため，ブレードは楕円を描くように平行移動する．このときの楕円のY_A方向の幅ΔYは10.8 (mm)，X_A方向の幅ΔXは9.2 (mm)であった．この楕円は屈曲関節中心間距離dが小さいほど小さくなるため，2自由度の屈曲関節において，dが小さいほど良い．

Fig. 4に示されるように，ブレード軸周りの回転角と本体軸周り回転角の差分$\Delta\gamma$は，ブレードの方向Z_Bと本体軸方向Z_Aの角度αが小さいほど，小さくなる．Fig. 5に示されるように，$\alpha=45$ (deg)の場合，$|\Delta\gamma|_{max}$は最大で19.8 (deg)である．従って，現実的に先端回転制御法を行うには，少なくともαの最大値が45 (deg)以下となるようブレードの方向Z_Bを制限する必要がある．

5. 結語

多自由度屈曲鉗子における先端回転制御法について数値シミュレーションを行い，USADブレードの方向が保たれ，$\alpha=45$ (deg)以下において，ブレード軸周りの回転が，本体軸周りの回転に，19.8 (deg)以下の差で追従可能であることを確認した．

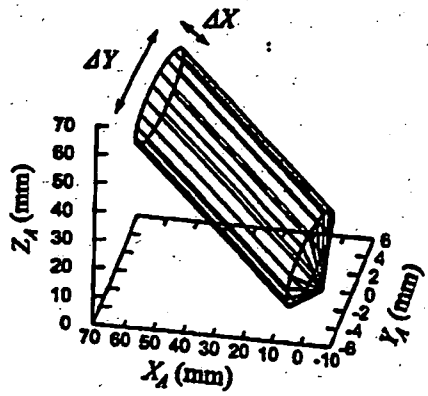

Fig. 3. Variation of position of the tip during the control of tip-rotation.

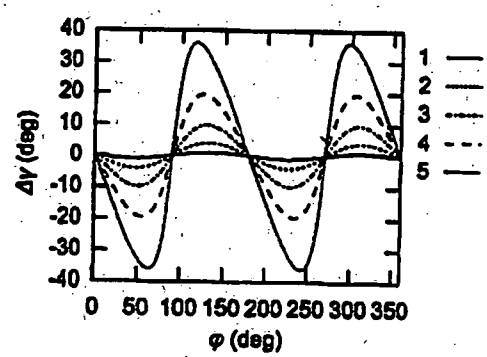

Fig. 4. Variation of $\Delta\gamma$. $\beta=0$ (deg); 1, $\alpha=15$ (deg); 2, $\alpha=30$ (deg); 3, $\alpha=45$ (deg); 4, $\alpha=60$ (deg); 5, $\alpha=75$ (deg).

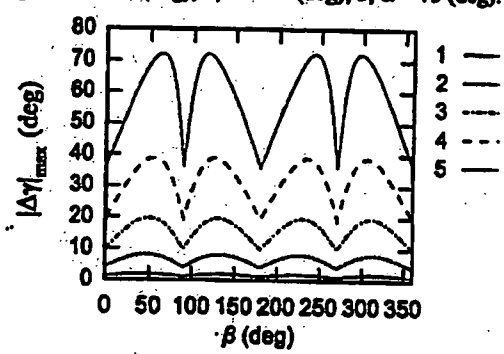

Fig. 5. Variation of $|\Delta\gamma|_{max}$. 1, $\alpha=15$ (deg); 2, $\alpha=30$ (deg); 3, $\alpha=45$ (deg); 4, $\alpha=60$ (deg); 5, $\alpha=75$ (deg).

謝辞

本研究の一部は文部科学研究費(#18680041)，成育医療委託研究事業(16 公-3)，および厚生科学研究費，身体機能解析・補助・代替機器開発研究事業(H15-フィジー-002)によるものである．

文献

1) Amaral JF, "The experimental development of an ultrasonically activated scalpel for laparoscopic use", Surg Laparosc Endosc , vol.4, pp.92-99, 1994

2) 中村 充一 他, "多自由度超音波凝固切開マニピュレータの開発—先端屈曲回転機構の開発と直感的インタフェースによるメカトロ駆動—", 日本機械学会ロボットメカトロニクス講演会 2007

(III)-12

超弾性合金を用いた多自由度屈曲鉗子の開発

○芦田 秀一[a], 小林 英津子[b], 佐久間 一郎[b]
[a]東京大学大学院新領域創成科学研究科, [b]東京大学大学院工学系研究科

Development of Multi-DOF Bending Forceps Manipulator using Superelastic Alloy

S. Ashida[a], E. Kobayashi[b], I. Sakuma[b]
[a] *Graduate School of Frontier Sciences, The University of Tokyo*
[b] *Graduate School of Engineering, The University of Tokyo*

bstract: Recently, Laparoscopic surgery is widely applied because of its minimal invasion. However, its operation is restrictive ecause it is necessary for surgeons to possess high surgical skills. To solve this problem, we have developed a wire driven ulti-DOF bending forceps using superelastic alloy for Laparoscopic surgery. In this study, we decided applicable length to ainless-superelastic integrated rod incorporated bending forceps. In addition, we proposed introduction of tension measurement ensors and algorithm to correcting backlash for giving better its operationality.

ey words: Laparoscopic surgery, Bending forceps, Superelastic alloy, Surgical robot

1. 背景

近年、開腹手術に代わる新たな手術方法のひとつとして腹腔鏡下手術が広く行われるようになってきた。しかし、術具が腹壁の挿入孔に拘束されることと、鉗子の自由度の低さのために、手術に相当の技術を要し、難しい手術に応用されていないのが現状である。

この問題点を解決するために、先端に把持機能しか持たない鉗子に屈曲自由度を持たせ、腹腔内で手技と同等の動きを実現する先端多自由度屈曲鉗子の開発が行われており[1]、我々はこれまで鉗子内部に超弾性合金を導入したワイヤ駆動の先端多自由度屈曲鉗子を開発してきた[1]。ワイヤ駆動方式は動力伝達系の剛性の低さと、その伸びのためのバックラッシによる動作精度と制御性の低さ等の多くの問題を抱えている。本研究では、ワイヤ駆動先端多自由度屈曲鉗子の問題の解決した超弾性合金を用いた新たな多自由度屈曲鉗子の開発を目的とする。

2. 方法

我々は機械的なワイヤ破断防止と張力リミットを目的として、動力伝達系のワイヤ経路内に超弾性合金—ステンレスロッドの一体型ロッドを導入した先端多自由度屈曲鉗子を開発してきた。しかし、超弾性合金は動力伝達用のステンレスワイヤに比べ剛性が弱く、ワイヤ経路内の伸びを抑制できていない。ワイヤ駆動に起因する問題点としては、①超弾性合金を含めたワイヤ経路の伸び、②張力不足によるワイヤのたるみ・バックラッシのばらつきがある。

そこで第1の問題を解決するために、一体型ロッド内の超弾性合金の割合を減らし、ワイヤ経路内の剛性を高くする。予備実験として超弾性合金長 100,75,50[mm]を含む試作機に導入している長さ 240[mm]の一体型ロッドについて、引張り試験を行い、その特性を調べ、超弾性合金の適切な長さを決めた。

また、第2の問題はワイヤに加わる張力がわからないため、ワイヤの初期張力不足や、張力のばらつきによって生じていると考えられる。そこでワイヤ経路内のプーリに加わる圧力からワイヤ張力を推定することで、上記を解消する。さらに、電気的な張力リミットとして用いることで安全性を向上し、張力を新たな制御パラメータとして導入することができると考えられる。

また、現状の先端関節機構ではワイヤが左右非対称に配置されており、張力のばらつきによる誤差を生じていた。そこで張力差による先端の誤差を減らすために、先端を両端支持の関節機構に改良した。(Fig1)

また、現状の鉗子ではバックラッシの累積による制御性の低下や、細かな屈曲動作が行えないといった問題が生じ

ている。それらを解消するためには、機構が大型化するがテンションプーリを導入して張力を一定に保つ等の必要がある[9]。そこで本研究では、回転方向とバックラッシ量を考慮したバックラッシ補正制御を導入する。これは回転方向に変化があった場合、現在地をバックラッシ分だけずれたとすることで、バックラッシ量の緩和をはかるものである。

3. 予備実験結果と考察

引っ張り試験機(Eztest,島津製作所)にて、超弾性合金とステンレスロッドを溶接にて結合した一体型ロッドの伸びと張力の関係を調べた. 一体型ロッドは超弾性合金長240,100,75,50[mm]の4種類について3[mm]までの伸びと張力の関係を調べた。

張力と伸びの関係(Fig.2)より、超弾性合金長を短くすることで、超弾性状態になるまでのモータの引き込み量を減らすことができた。しかし、100,75,50[mm]では大きな差が得られなかった。そこで一体型ワイヤ内の超弾性合金の張力と歪の関係(Fig3)を見ると超弾性合金は一定のヤング率を示していないことがわかる。超弾性合金の適切な長さを決める要因としては"一体型ロッド全体の伸びが少ないこと"と"超弾性合金部の歪が極力少ないこと(1～2%程度)"があげられる。Fig3より、2%程度で十分に超弾性域に到達する100[mm]が妥当であると考えられる。

4. 結論

ワイヤ駆動先端多自由度屈曲鉗子において、内部に導入する一体型ワイヤにおいて、超弾性合金の適切な長さを検討するため、合金長を変えた一体型ロッドについて引張り試験を行い、超弾性合金長を決定した。また、ワイヤ張力のばらつきを抑えるために先端の構造を改良した。今回決定した超弾性合金長の一体型ロッドと、張力センサを内蔵した鉗子を製作し、バックラッシ補正を導入し手持ちデバイスとして、動物実験によりその操作性を評価を行う。

謝辞

本研究の一部は厚生科学研究費、身体機能解析・補助・代替機器開発研究事業(H15-フィジー-002)によるものである。

参考文献

1) 芦田 秀一, 他6名, 超弾性合金を用いた多自由度屈曲鉗子マニピュレータ機構の改良, 第4回生活支援工学系学会連合大会論文予稿集, p.78, 2006

2) K.Ikuta, et al, "Hyper-finger for Remote Minimally Invasive Surgery in Deep Area", Medical Image Computing and Computer-Assisted Intervention (MICCAI'02), pp.171-181('part 1), 2002

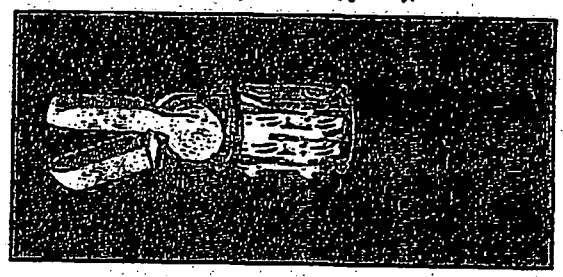

Fig.1 Tip mechanism

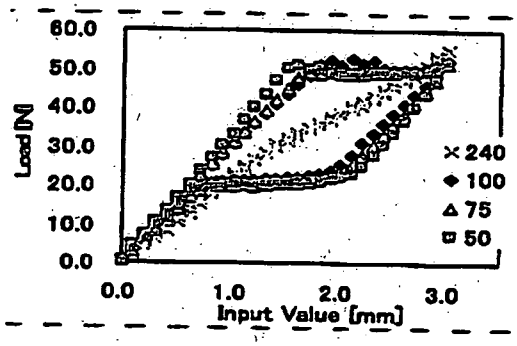

Fig.2 Load-extension diagram

(Integrated rod)

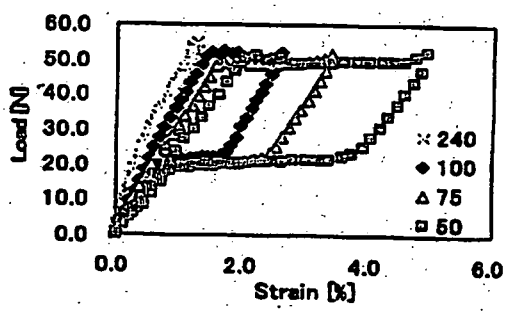

Fig.3 Load-strain diagram

(Superelastic alloy)

07(XI)-48 脳神経外科手術支援のための手術ナビゲーションシステムに関する研究

○王 凱鳴[a]，安藤 岳洋[a]，島谷 浩二[a]，野口 雅史[a]，青木 英祐[a]，
廖 洪恩[a]，小林 英津子[a]，丸山 隆志[b]，村垣 善浩[b]，伊関 洋[b]，佐久間 一郎[a]
[a]東京大学，[b]東京女子医科大学

Research of the surgical navigation system for a neurosurgery

Kaimeng.WANG[a], Takehiro.ANDO[a], Koji.SHIMAYA[a], Masafumi.NOGUCHI[a], Eisuke.AOKI[a],
Hongen.LIAO[a], Etsuko.KOBAYASHI[a], Takashi.MARUYAMA[b], Yoshihiro.MURAGAKI[b], Hiroshi.ISEKI[b]
and Ichiro.SAKUMA[a]
[a]*The University of Tokyo*, [b]*Tokyo Women's Medical University*

Abstract: In neurosurgery such as the treatment of glioma, it is important to remove tumor accurately. Obscure boundaries between normal tissue and glioma prevent surgeon from detecting easily. Navigation system has been used in a clinical operation to help surgeon detect brain tumor easily. But there is a special phenomenon called "Brain shift", which is deformation and translation of brain in a clinical operation.5-Aminolevulinic Acid(5-ALA), a tumor-marker with fluorescence, is used for assisting intra-operative detection of brain tumor and its boundaries. We developed the measurement system using 5-ALA for assisting intra-operative detection of brain tumor. It is necessary, however, to integrate intra-operative information acquired from a various surgical measurement systems with preoperative information for effective surgical navigation. In this research, we developed an integrated intra-operative information system consisted of navigation system, and intra-operative measurement system using 5-ALA.

Key Words: 5-ALA, Brain tumor, System integration, Navigation system, Neurosurgery

1. 背 景

脳腫瘍の治療としては全摘出が最も有効な治療法であり，腫瘍の除去率と患者の予後には密接な関係がある．しかし，悪性腫瘍は浸潤性を持ち，正常組織との境界が不明瞭であるため，腫瘍，非腫瘍の境界を判断することが難しく，また，過度の摘出は患者の予後にも影響を与えますから，実際の症例で全摘出といえるのはわずかしかないという現状がある．そのため正確な腫瘍摘出が求められており，腫瘍領域を把握するMRIなどの診断装置や，それと合わせて腫瘍の空間情報を術者に直感的に提示するナビゲーションシステムなどが開発されている．しかしながら，術中には髄液の流出により脳が変形・移動するブレインシフトという現象が見られ，腫瘍の部位は術前画像と術中において必ずしも一致しない．この問題の解決法としては術中MRIの応用等がある．また腫瘍同定のための術中計測も有効であると考えられる，このような試みのひとつとして腫瘍細胞に選択的に集積し，蛍光色素Protoporphyrin IX(Pp IX)の前駆体である，5-Aminolevulinic Acid(5-ALA)を利用して腫瘍組織と正常組織との識別を行う試みがなされている[1]．我々は腫瘍部位で計測される蛍光信号の強度・蛍光スペクトルと腫瘍の性質に関する情報(術中の腫瘍の種別及び悪性度など)を検討を行い，術中腫瘍部位同定支援のための5-ALA誘導蛍光術中計測システムの開発を行っている．この計測システムから得られる組織診断に関する情報を，直感的かつリアルタイムに手術ナビゲーション画面に提示可能になれば，術中に状況に応じた最適な手術戦略立案の支援ができる．しかしながら，臨床ではMRI等の診断装置と組み合わせたナビゲーションシステムの利用は盛んに行われているものの，術中に計測される脳腫瘍術中計測診断システムから得られる組織機能情報が統合されたシステムが必要である．

2. 目 的

本研究では術中計測情報と手術ナビゲーションシステムを統合した手術支援システムを開発する．具体的には以下の二点を検討する．

1、5-ALAを利用した術中計測システムと位置計測ナビゲーションシステムを統合する．

2、術中計測システムから得られた蛍光スペクトル情報をナビゲーション上に提示する方法を検討する．

3. システム構成

システムの概要をFig.1に示す．統合するシステムは，術中の腫瘍同定に役立つPpIX蛍光計測システム，それを搭載し術場に置かれるこれらの計測デバイスの3次元位置情報を計測し，位置情報統合（レジストレーション）を行うための位置計測を行う3次元位置計測システム，これらを統合して術者に直感的な情報として提示するナビゲーションシステムから構成される．これらのサブシステム間のデータの送受信はMiddle Ware(NDDS)[2]によって行われる．

Fig.1 System architecture of integrated intra-operative information system

このシステムに実装する機能は以下の通りとした．

(a)計測された点の位置情報（三次元計測装置座標系）とMRI画像とを統合する．

(b)取得された蛍光情報をナビゲーション上に提示する．

(c)データベース機能を付加する．類似度の近いスペクトルの検索し，類似度の近いスペクトルを提示し，腫瘍の判別を行う．

各拡張機能の実装は，3D Slicerをベースに行った．

4. 実験

4.1 座標系統合評価

座標系の統合評価を行うために，MRIで撮像可能な非磁性体のアクリル製の容器を使った．MRI座標系と光学式位置計測装置(OTS)座標系で計測されたR,S,Q,rの4点で作られる座標値から，MRI座標系を基準としてOTSを用いた座標計測値の比較を行った．A,B,C,D,R,S,Q,r,s,qの計測から算出されたナビゲーションのTRE誤差は平均2.22mmであった．

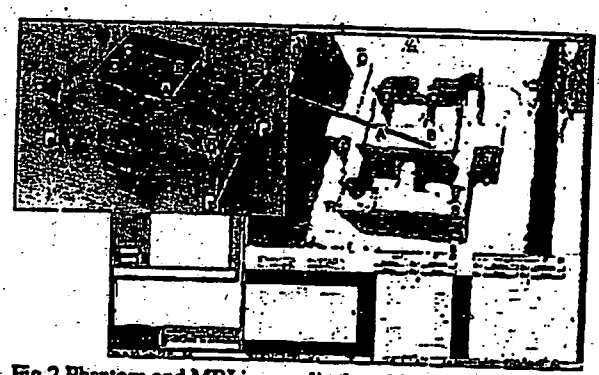

Fig.2 Phantom and MRI image displayed in 3D Slicer

4.2 情報統合システム

ハンドプローブ型の組織蛍光計測プローブに反射型の光学式マーカを取り付け，Fig.1のような統合環境下にて，取得した蛍光強度及び位置情報を送信し，ナビゲーションシステムとの連動実験を行った．術者が指し示した蛍光発生箇所を位置情報とともにナビゲーション画面上にて提示を行うことが可能であった(Fig.3)．

Fig.3 Experimental results of navigation system

5. まとめと今後の展望

5-ALA誘導蛍光計測にもとづく術中腫瘍同定のための計測情報と，手術ナビゲーションシステムを統合した術中情報提示システムを試作した．有効な情報提示の手法を今後検討する必要がある，また，臨床例で計測された5-ALA誘導蛍光と病理診断結果をまとめたデータベースを試作し，組織蛍光スペクトル波形の過去の臨床例との相関性から，腫瘍、境界と非腫瘍の判別を支援する手法の検討を行う．

「本研究の一部は厚生科学研究費，身体機能解析・補助・代替機器開発研究事業（H15-フィジ-002)による．」

文献

1) Walter Stummer: Neurosurgery, 42, (3), 518-526 (1998).

2) E.Aoki. et.al, Development of an intraoperative information integration system and implementation for neurosurgery,Journal of Robotics and Mechatronics, vol.19, no2, pp.339-352

07(XIV)-58

5-ALA 誘導 PpIX蛍光を用いた術中局所的脳腫瘍識別システムに関する研究

○安藤 岳洋[a], 島谷 浩二[b], 野口 雅史[b], 小林 英津子[a], 丸山 隆志[c], 村垣 善浩[d], 伊関 洋[c,d], 佐久間 一郎[a]

[a]東京大学 大学院工学系研究科, [b]東京大学 大学院新領域創成科学研究科,
[c]東京女子医科大学脳神経外科
[d]東京女子医科大学 大学院先端生命医科学研究所先端工学外科

Intraoperative Local Demarcation System of Brain Tumor for 5-ALA induced Porphyrins

T.Ando[a], K.Shimaya[b], M.Noguchi[b], E.Kobayashi[a], T.Maruyama[c], Y.Muragaki[c], H.Iseki[c], I.Sakuma[a]

[a]*Graduate School of Engineering, The University of Tokyo*
[b]*Graduate School of Frontier Sciences, The University of Tokyo*
[c]*Department of Neurosurgery, Neurological Institute, Tokyo Women's Medical University*
[d]*Faculty of Advanced Techno-Surgery, Institute of Advanced Biomedical Engineering and Science, Graduate School of Medicine, Tokyo Women's Medical University*

Abstract: 5-Aminolevulinic Acid (5-ALA), a metaboric precursor of protoporphyrin IX (PpIX) has recently been used for intraoperative demarcation and visualization of glioma tissues. It is necessary for complete resection of Malignant glioma to improve the fluorescence detection system that has high sensitivity and high-resolution ability. We have previously developed a handheld device for localized identification system of brain tumor with the measurement resolution 0.6mm. However, precise positioning was required for stable measurement of fluorescence. Furthermore, the size and weight were still large. It was difficult to hold the device during a measurement and to keep the appropriate distance from the target point. We developed the new pen-like fluorescence detection probe that had high sensitivity, high-resolution ability and lightweight. Resolution ability that is investigated using white-black seat and precision positioning stage was 0.5mm at 7.0mm distance between sample and probe.
Key words: 5-ALA, ProtoporphyrinIX, Brain Tumor, Fluorescence Detection

1. 背景

Glioma をはじめとする悪性脳腫瘍の治療において、腫瘍の摘出率は患者の予後に密接に関係している。しかし、悪性脳腫瘍は正常な脳組織に浸潤しながら成長するため、腫瘍部位を肉眼で正確に特定することが困難である。そのため、腫瘍に選択的に蓄積して蛍光物質に変化する 5-Aminolaebrinic Acid(5-ALA)を用いた脳腫瘍同定法が考案されてきた[1]。しかし、それらは目視によって蛍光を観測していたため、微小な腫瘍部位を取り残す可能性がある。この問題を解決するには高い空間分解能を持ち、感度のよい蛍光検出システムが必要とされる。

これまでの研究で、吸入管をベースにした術者手持ち型の蛍光計測システムが考案された。このシステムは空間分解能 0.6mm を有するが[1]、蛍光励起レーザ光学系と蛍光検出光学系が独立に置かれており、蛍光励起レーザビームと検出プローブの測光領域が重なった狭い領域に計測可能点が限定されていたため、プローブの細かな位置決めが必要であった。このため計測可能領域から目的とする計測点がわずかでも外れてしまうとほとんど蛍光を検出出来なくなってしまうという問題点があった。また、レーザーモジュールも測定プローブに付属しているため、重量が重く、外形寸法も大きいため術者にとって重く持ちにくいものであった。本稿では、これらの問題を解決した手持ち型局所的脳腫瘍同定システムの開発とその性能評価について報告する。

2. システム構成

本研究で開発したシステムは、5-ALA の励起光用の波長 405nm レーザーと蛍光検出用の分光器、そして励起と蛍光検出を同時に行うためのプローブからなる。プローブは、1 本の蛍光検出用ファイバの周りに 6 本の励起光用ファイバが束ねられたバンドルファイバと集光用のレンズ系から構成されている(Fig.1)。それぞれのファイバのコア径は 400 μm、NA は 0.22 である。

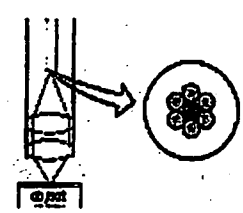

Fig.1 Laser-induced fluorescence detection probe

先端の光学系は、拡散する励起光を集光すると同時に、微小領域の蛍光を効率よくファイバに導光することを目的として設

計されている。レンズは二枚のアクロマートレンズ(φ9.0mm)から構成され、ファイバ端面側のレンズの焦点距離は 18.0mm、対物側のレンズの焦点距離は 12.0mm である。このレンズ系の倍率は 1.5 倍、NA=0.35 である。これより、MRI 画像の空間分解能(1mm)以上の性能を持ち、ファイバ単体よりも光量取得効率のよい計測系を目標とした。

これらを収めたプローブは、重量:45g (ファイバは除く)、外径:φ11mm、全長:250mm であり、材質はステンレスとアルミで構成されている。

3. 評価実験

3.1 分解能評価実験

本研究で開発した蛍光検出用プローブの空間的検出分解能を測定するために、0.002mm の微動が可能なメカニカルステージに試料(白黒シート)を固定し、それと垂直にプローブを設置し、励起光を照射して試料表面の境界をまたぐように直線的に走査した。走査区間は 10mm とし、0.1mm ごとに分光器でスペクトル情報を記録して波長 430nm 周辺のピーク値を輝度値として使用した。得られた位置と輝度値の情報を Savitzky[2]の方法を用いて2次微分を算出し、正負のピークを持つ点の幅をプローブの観察している領域(空間分解能)とした。2次微分値の負のピークは信号の変化の始点を、正のピークは終点を表すものとして評価した。この実験をプローブの端面と試料の距離を 3.5～13.5mm に 0.5mm 刻みで変化させてそれぞれの距離について測定を行った。

また、分解能の向上と光量取得効率の向上をファイバ単体の場合と比較するために、レンズ系を取り除いた場合(ファイバ単体)についても評価実験を行った。

3.2 輝度値の変化の計測

プローブ端面からの距離によって取得できる光量がどの程度変化するかを調べるために、プローブの端面と試料の距離を 3.5～13.5mm の間で 0.5mm 刻みで変化させ、波長 430nm 周辺のピーク値を輝度値として記録した。これについてもレンズ系がある場合とない場合を比較するために、それぞれについて輝度値の変化を記録した。

4. 結果

レンズ系がある場合とない場合のそれぞれについて分解能評価実験を行った結果を Fig.2 に示す。レンズ系がない場合、分解能は端面からの距離が離れるにしたがって低くなっているが、レンズ系がある場合は焦点付近(distance=7～9mm)において分解能が最高になっている。そのときの分解能は 0.5mm 以下を達成している。また、端面から 3.5～5mm まではレンズ系を装着しないほうが分解能は高いが、5～13.5mm ではレンズ系があるほうが分解能は高い。

プローブ端面からの距離の変化に対する輝度値の変化を測定した結果を Fig.3 に示す。プローブ端面から 3.5～5.5mm の区間ではファイバ単体のほうが取得光量は大きいが、5.5～13.0mm の区間ではレンズ系があるほうが取得光量は大きかった。

これらの結果より、開発したプローブは端面と試料の距離が 7mm の場合において分解能、取得光量ともに最良となることがわかった。また、そのときの分解能、輝度値ともにレンズ系がない場合に比べて約 3 倍となっている。

7. 結語

小型化・軽量化を図り術者が把持しやすく空間的分解能が高い、5-ALA 誘導 PpIX 蛍光術中検出用プローブを試作した。試作したプローブにおいてレンズ系がある場合とない場合とで分解能と取得光量を計測、レンズ系がある場合は、分解能、取得光量ともにレンズ系がない場合を約 3 倍上回った。

本研究の一部は厚生科学研究費、身体機能解析・補助・代替機器開発研究事業(H15-フィジ-002)による。

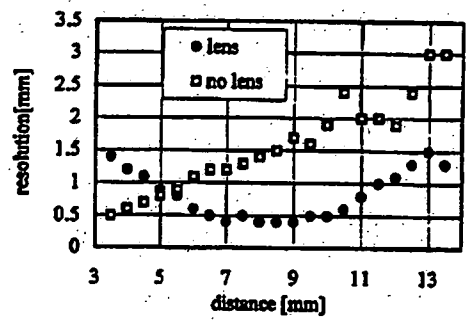

Fig. 2 Optical resolution of probe (with lens, with no lens)

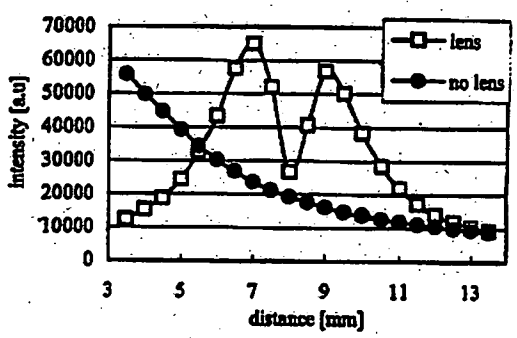

Fig.3 Transition of acquiring intensity (with lens, with no lens)

文献

1) W.Stummer et al; Fluorescence-guided resection of gliobrastoma multiform by using 5-aminolevulinic acid-induced porphyrins: a prospective study in 52 consecutive patients, J Neurosurg, 2000
2) Abraham Savitzky, et al, Smoothing and Differentiation of Data by Simplified Least Squares Procedures, Analytical Chemistry, 36, 1627-1639, 1964
3) 吉田大樹 他. 5-Aminolevelinic Acid 誘導蛍光による術中脳腫瘍同定のための蛍光局所計測法に関する研究. 第14回日本コンピュータ外科学会大会論文集, 千葉, pp.97-98, 2005

07(XIV)-63

MRI 誘導下手術支援マニピュレータにおける同期制御を用いた MRI 対応性の基礎検討 (第 2 報)

[a] 鈴木孝司, [b] 廖洪恩, [b] 小林英津子, [b] 佐久間一郎
[a] 東京女子医科大学 先端生命医科学研究所, [b] 東京大学 工学系研究科

Preliminary trial of a novel MRI compatible method based on synchronized control for MRI-guided surgery-assisting robotic manipulator (2nd report).

[a]Takashi Suzuki, [b]Hongen Liao, [b]Etsuko Kobayashi, [b]Ichiro Sakuma
[a]*Institute of Advanced Biomedical Engineering and Science, Tokyo Women's Medical University,* [b]*Graduate School of Engineering, The University of Tokyo*

Abstract: Integration of surgery-assisting manipulator and magnetic resonance (MR) image-guided surgery will provide sophisticated surgery by enhancing surgeons' dexterity and diagnostic ability. Electromagnetic noise from actuator and sensor of manipulator, however, degrades the quality of MR images. We have introduced a novel motor control method that actuates ultrasonic motor synchronously during "dead time" in scanner's pulse sequence not to interfere image signal acquisition. The 1st report showed the feasibility of noise reduction by synchronous motor control. In this study, we report the variation of signal-to-noise ratio (SNR) depending on the distance from center of magnet. In evaluation tests, ultrasonic motor was located at the distance of 200, 350, 500 mm from the center of magnet. Imaging phantom was scanned using fast spin echo/gradient echo while motor was actuated continuously/synchronously. SNR was calculated from acquired images. Though in the cases of 200, 350 mm, continuous actuation decreased the SNR, in the case of 500 mm, SNR of synchronous motion was not below that of continuous one. The results showed synchronous actuation is valid regardless of distance from center of magnet, and distance separation is sometimes not enough measure.

Key words: Magnetic resonance imaging, Intraoperative MRI, Image-guided surgery, Surgical manipulator, Piezoelectric ultrasonic vibration motor, Electromagnetic noise, Synchronous control.

1. 背景

術中に核磁気共鳴画像 (Magnetic Resonance Image, MRI) を取得し，最新の情報を用いた手術計画の更新，その計画に基づいた手術支援マニピュレータの駆動が研究されてきた [1]．しかし，MRI 環境下では MRI 対応性 [2] が必要であり，マニピュレータの部品の選定には注意を要する．MRI 対応モータの一つとして超音波モータがある．非磁性材料の使用により磁場からの吸引力や静磁場の歪みについては対応可能だが，モータ駆動時に発生する電磁波ノイズが画質を劣化させる [3]．対策としてモータの電源遮断 [1]，MRI から離れた場所へのモータの設置 [4,5]，バンドパスフィルタの使用 [6] 等が試みられたが，操作の煩雑化，駆動力の伝達機構による装置の大型化，周波数依存のノイズ低減特性といった欠点もあった．そこで撮像シーケンス中の緩和時間のうち信号を取得しない時間 (dead time) に限定してモータを駆動することで，MRI 装置とモータ駆動の干渉を避ける方法を提案した [7,8]．Zhang らの研究では MRI 装置との同期制御に MRI 装置から出力されるタイミング信号を用いたが，これはハードウェア依存であり汎用的ではない．そこで撮像の一つの時間単位である繰返時間 (Repetition Time, TR) 開始時点で発振される RF 信号を同期トリガとして受信し同期を実現した．本報告ではガントリ内でモータの位置によらず本手法の有効性を確認した．

2. 方法 [8]

本手法ではパルスシーケンス内の dead time を用いる (Fig. 1)．この時間には MRI 装置は信号受信を停止するためノイズ発生があったとしても画像信号との干渉が無く画質が劣化しない．この時間に限定してモータを駆動するためには MRI 装置とモータ駆動系との同期が必要である．その同期トリガとして TR 開始時点で発振される RF 信号を用いた．LC 共振回路を用いた自作のアンテナにより RF 信号を受信し，波形整形を行った後，コンピュータに入力する．入力があった段階でモータ駆動系の時間軸をリセットすることで各 TR 開始時点で同期を行う．

3. 評価実験

本手法は撮像空間からの距離ではなく時間的な切り分けにより，ノイズ削減を実現している．つまりモータの設置位置によらず本手法が有効に機能することを信号対雑音比 (signal-to-noise ratio, SNR) を用いて評価した．

実験には開放型ガントリを有する垂直磁場タイプの実験用 MRI 装置を使用した．磁場中心に設置した頭部用コイル内に撮像用ファントム (NaCl, $NiCl_2$ 水溶液) を設置した．超音波モータ (USR60-E3N, 新生工業) を磁場中心から 200 mm(コイル端), 350 mm, 500 mm に設置した (Fig. 2)，モータの電源が off/on の場合，そして同期駆動/連続駆動を行った場合について 5 回ずつ画像を取得し，その SNR の平均を比較した．撮像シーケンスは fast spin echo(FSE)(TR/TE=400/15 msec, ESP=15 msec,

ETL=8, FA=90 deg, 解像度 128×128) および gradient echo(GE)(TR/TE=100/15 msec, FA=65 deg, 解像度 128×128) を用いた.

モータを導入せずファントムのみを撮像した場合を基準として, SNR の低下を Fig. 3–4 に百分率で示した. 電源 off と比べて, 電源 on, 同期駆動をした場合は SNR は変化しないが, 連続的にモータを駆動した場合は SNR の低下が見られ, 磁場中心に近づくほど顕著になっている. モータを y=500 mm に設置したとき SNR の低下が最小となり約 10% であった. 我々の予備実験から 10% 程度の SNR の変化は誤差範囲であることがわかっており, 500 mm の距離をおくことでノイズの問題は防げるとした先行研究[4,5]と一致したが, それ以外の方向へ 500 mm 離して設置した場合には SNR の低下が見られるため, 500 mm の距離が必ずしも十分ではないことが示された.

4. 結論

MRI 下で超音波モータ駆動時に問題となるノイズに対して, 一対策法として撮像シーケンス内の dead time を用いたモータ駆動法を提案し, その手法がガントリ内でモータの設置位置によらず有効であることを示した.

謝辞

本研究の一部は厚生労働科学研究費補助金 (身体機能解析・補助・代替機器開発研究事業)「新たな手術用ロボット装置の開発に関する研究」によるものである.

文献

1) K.Masamune, et al. Development of an MRI-compatible needle insertion manipulator for stereotactic neurosurgery. *J Image Guid Surg*, 1 (4): 242–248, 1995.
2) GE Medical systems. MR Safety and MR Compatibility: Test Guidelines for Signa SP^{TM}. Version1.0., 1997.
3) Y.Koseki, et al. Endoscope manipulator for trans-nasal neurosurgery, optimized for and compatible to vertical field open MRI. *MICCAI2002*, 114–121, 2002.
4) 岸宏亮他. MRI 環境対応小型手術支援 7 自由度マニピュレータの開発. *ROBOMEC2006*, 2A1–A15, 2006.
5) 神垣剛他. 前立腺がん MR 誘導下収束超音波治療におけるプローブ操作のための MR 対応材料性マニピュレータの開発. *J JSCAS*, 8 (3): 93–94, 2006.
6) T.Oshiro, et al. Reduction of electronic noise from radiofrequency generator during radiofrequency ablation in interventional MRI. *J Comput Assist Tomogr*, 26 (2): 308–316, 2002.
7) Q.Zhang, et al. A method for simultaneous RF ablation and MRI. *J Magn Reson Imaging*, 8 (1): 110–114, 1998.
8) 鈴木孝司他. MRI パルスシーケンスとの調和性を考慮した MRI 対応性に関する基礎検討. 生体医工学, 44 (4): 728–734, 2006.

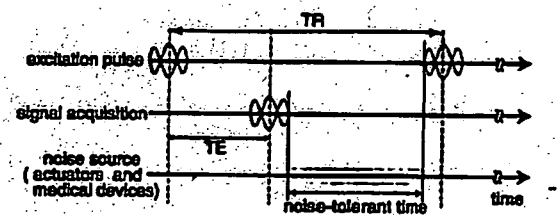

Fig. 1 Synchronization method using RF pulse as a trigger at the start point of repetition time (TR).

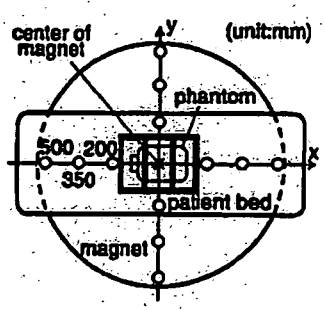

Fig. 2 Motor was set at the distance of 200, 350, 500 mm from the center of magnet.

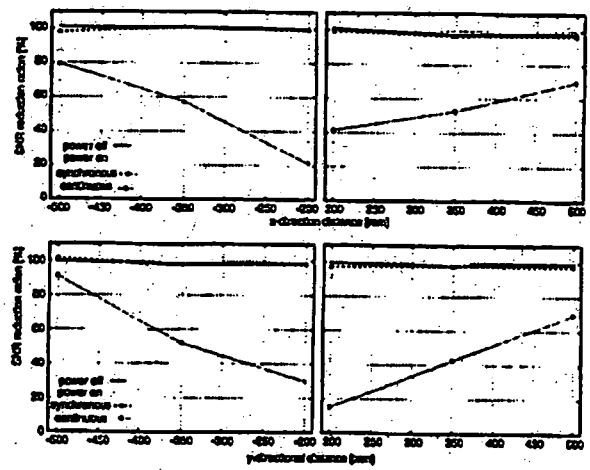

Fig. 3 Decrase of SNR in FSE scan.

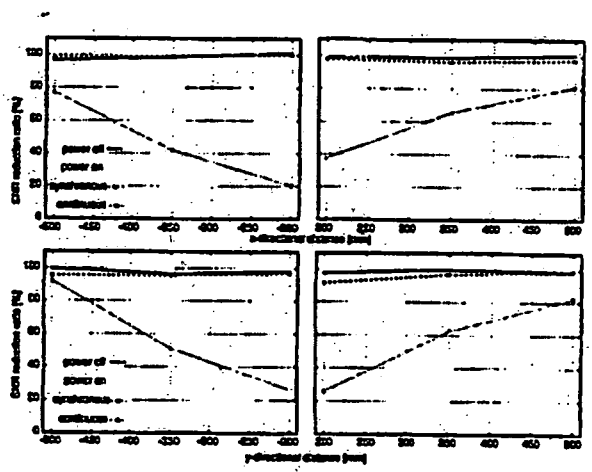

Fig. 4 Decrase of SNR in GE scan.

07(XIV)-69

5-ALA誘導型PpIXによる蛍光画像を用いた脳腫瘍の術中同定に関する研究

○島谷 浩二[a], 野口 雅史[a], 小林 英津子[a], 丸山 隆志[b], 村垣 善浩[c], 伊関 洋[b,c], 佐久間 一郎[a]

[a]東京大学大学院新領域創成科学研究科, [b]東京女子医科大学脳神経外科,
[c]東京女子医科大学大学院先端生命医科学研究所先端工学外科分野

The Method utilizing fluorescent images of 5-Aminolevulinic Acid-Induced PpIX for Intra-operative Brain Tumor Detection

K. Shimaya[a], M. Noguchi[a], E. Kobayashi[a], T. Maruyama[b], Y. Muragaki[c], H. Iseki[b,c], I. Sakuma[a]

[a] *Graduate School of Frontier Science, The University of Tokyo*
[b] *Department of Neurosurgery, Neurological Institute, Tokyo Women's Medical University*
[c] *Faculty of Advanced Techno-Surgery (FATS), Institute of Advanced Biomedical Engineering and Science, Graduate School of Medicine, Tokyo Women's Medical University*

Abstract: 5-Aminolevulinic Acid (5-ALA) turns into a fluorescent substance called ProtoporphyrinIX (PpIX) when administered to a living body. PpIX is especially accumulated in pathological lesion, excited by blue light and emits red fluorescence by which we can know the existence of tumors. The fluorescence can assist to detect malignant brain tumors and brain regions can be visualized with a procedure of CCD camera intra-operatively, and removal rate of tumor can be improved. In this study, spectrums of human brain tissues were obtained in vitro, and fluorescent properties of malignant tumor and non-tumor tissues were acquired. By utilizing this finding, we proposed optical filters and methods using fluorescent images obtained by using CCD camera for discriminating tumor regions. One method is based on discriminant analysis method, and another utilizes clustering algorism. We made a phantom simulating optical properties of brain tissues, and those methods were compared and evaluated by using this phantom.

Key words: 5-Aminolevulinic Acid, ProtoporphyrinIX, Brain tumor, CCD camera, Fluorescent image, Discriminant analysis method, Clustering algorism

1. はじめに

悪性脳腫瘍の治療法として外科的な腫瘍摘出手術は最も有効な治療法の一つであり，除去率と患者の予後には密接な関係がある．そのため，できる限り摘出することが望ましいが，悪性脳腫瘍は浸潤性を持ち，正常組織との境界が不明瞭なためその判断が困難である．また，過度な切除は脳機能の損失に繋がる危険性がある．そのため腫瘍細胞に選択的に集積し，蛍光色素 ProtoporphyrinIX(PpIX)の前駆体となる5-Aminolevulinic Acid(5-ALA)を用いて，腫瘍組織と正常組織との識別を行う試みがなされている[1]．5-ALA は術前に患者に投与されると励起光の照射により蛍光を発生し，これによって術中に腫瘍部位の確認が可能である．先行研究ではカメラと光学フィルタを用いて広領域での腫瘍同定を行っている[2]が，腫瘍部位に隣接した正常組織も過度に摘出している．これは正常組織からも蛍光が発生されている可能性があることが原因であり，蛍光発光部位を描出するだけでは不十分だと考えられる．そこで本研究では摘出した脳組織の蛍光スペクトルを計測し，その計測結果に基づき腫瘍部位のみを同定するための光学フィルタと同定手法を提案し，その評価を行った．

2. 方法

2.1. 蛍光スペクトル計測

5-ALA を投与した患者の手術において摘出された脳腫瘍組織に波長 405[nm]，15[mW](CW)の青紫色半導体レーザ（φ5[mm]，コリメートビーム）による励起光を照射し，光ファイバと小型分光器を用いて蛍光スペクトルを測定した．Fig1 は代表的な腫瘍，及び非腫瘍組織の蛍光スペクトルである．腫瘍組織からの蛍光は 635[nm]付近にピークを持っており，また非腫瘍組織は腫瘍組織と比較すると微弱ではあるが 580，628[nm]付近にピークを有していた．また PpIX由来の蛍光スペクトルの立ち上がりの波長は 620[nm]付近であった．(Fig1)

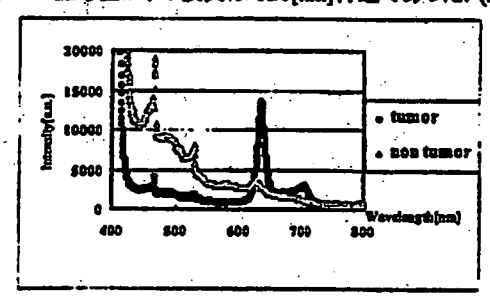

Fig.1 Spectrum of the tumor and non-tumor tisuue

2.2. 蛍光画像計測

(a) 脳組織を模擬したファントム

脳組織の蛍光特性，及び散乱特性を模擬したファントムを作成する．腫瘍組織の蛍光特性はPpIXを 4[μg/ml]，非腫瘍組織はPpIXを0.168[μg/ml]，Flavin を16[μg/ml]加えることによ

り模擬した．また静注用脂肪乳剤Intralipid10[%]を用い，文献[3]に基づき腫瘍，非腫瘍組織の散乱特性を再現した．寒天で溶液を半固形状にすることで腫瘍，非腫瘍層を作成し励起光を照射して蛍光画像を取得した．

(b) 腫瘍同定手法

摘出された腫瘍，非腫瘍組織の蛍光特性に基づき Cut-off 波長 550[nm], 620[nm]の Long pass filter(LPF), 及び中心透過波長 636[nm], FWHM10[nm]の Band pass Filter(BPF)を用いて，ファントムの蛍光画像を取得した．本研究では蛍光発光部位を腫瘍と非腫瘍の2つのクラスにクラスタリングし腫瘍部位を同定する手法として，以下の2つの手法を提案しそれらの手法の比較，及び評価を行う．

(i)1枚の蛍光画像の輝度値を特徴量として，判別分析法[4]に基づいた自動閾値選定法により閾値を選定し，閾値以上の画素を腫瘍とみなす

(ii)Cut-off 波長 550[nm], 620[nm]の LPF により取得した蛍光画像の差分画像の輝度値を特徴量1，Cut-off 波長 620[nm]の LPF の輝度値を特徴量2とした特徴空間上において，先ず K-means 法を用いて 2 つのクラスの重心座標を計算する．次に，計算した重心座標を初期値として EM アルゴリズムにより2次元での混合正規分布を推定し，各画素について腫瘍部位に対する所属確率が 0.5 以上である画素を腫瘍とみなす．

各蛍光画像の輝度分布，及び手法(i)によりファントム上で腫瘍部位とみなした領域を抽出した結果を Fig2, Fig3 に示す．また手法(ii)を用いた際における特徴空間上での確率分布を Fig4，画像上での各画素の腫瘍のクラスに対する所属確率，及び腫瘍部位とみなした領域を抽出した結果を Fig5 として示す．

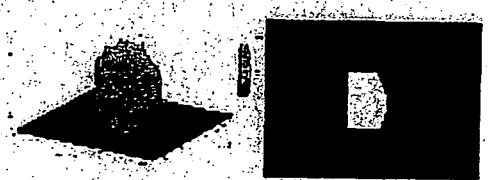

Fig.2 Intensity of the fluorescent image and the result of detecting tumor region on phantom by using LPF with cut-off 620[nm]

Fig.3 Intensity of the fluorescent image and the result of detecting tumor region on phantom by using BPF with center wavelength of transmission 636[nm] and FWHM 10[nm]

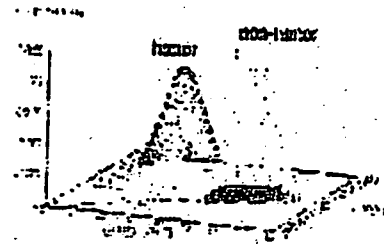

Fig.4 Probability distribution in feature space

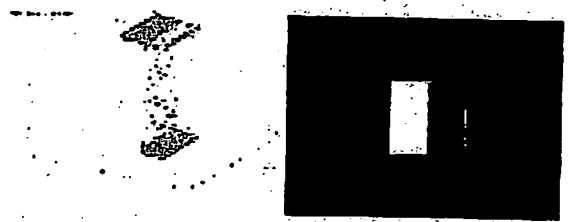

Fig.5 Probability belonging to tumor region in the fluorescent image and the result of detecting tumor region

3. 考察，及び結語

手法(i)により腫瘍部位とみなした領域を抽出した場合，境界部分を境に，ファントム上での腫瘍層を明確に抽出できていないことがわかる．これは空間上での励起光の強度にむらがあり，特に中心部分において強度が大きいことが理由である．一方，手法(ii)を用いた場合，境界部分を境に腫瘍層を抽出できてはいるが，非腫瘍層の周辺部分も誤って腫瘍とみなし抽出している．これは腫瘍と非腫瘍にクラスタリングした際に，特徴空間上での原点付近，つまり輝度が比較的小さい画素を腫瘍のクラスにクラスタリングしたことが原因であると考えられる．

また提案した2つの腫瘍同定手法の評価方法として，定性的ではあるが，先ずファントム上の腫瘍層の pixel 数を計算し，これを正解の pixel 数とした．次に各手法により腫瘍部位とみなし抽出した領域の pixel 数を計算し，正解の pixel 数との比較を行った．Cut-off 波長 620[nm]である LPF を用いて蛍光画像を取得した場合，中心透過波長 636[nm]である BPF を用いて蛍光画像を取得した場合はそれぞれ 1.25 倍，1.03 倍であった．また手法(ii)を用いた場合は 1.09 倍であった．

今回はファントムを用いて提案手法の評価を行ったが，今後は摘出された脳組織を用いて，各提案手法の比較を行う予定である．

文献

1.) Walter Stummer, et al., Intraoperative detection of malignant gliomas by 5-aminolevulinic acid-induced porphyrin fluorescence, Neurosurgery Vol.42, No3, p518-526, 1998

2.) Arjen Bogaards et al., Increased Brain Tumor Resection Using Fluorescence Image Guidance in a Preclinical Model, Lasers in Surgery and Medicine Vol.35, p181-190, 2004

3.) Toms Steven et al., Intraoperative Optical Spectroscopy Identifies Infiltrating Glioma Margins with High Sensitivity., Neurosurgery. 57(4), 382-391, 2005

4.)大津展之，判別および最小 2 乗基準に基づく自動しきい値選定法，電子通信学会論文誌，J-63D, 349-356, 1980